ACS APPLIED MATERIALS & INTERFACES

Research Article

www.acsami.org

MnO_2-Nanosheet-Modified Upconversion Nanosystem for Sensitive Turn-On Fluorescence Detection of H_2O_2 and Glucose in Blood

Jing Yuan, Yao Cen, Xiang-Juan Kong, Shuang Wu, Chen-Liwei Liu, Ru-Qin Yu, and Xia Chu*

State Key Laboratory of Chemo/Biosensing and Chemometrics, College of Chemistry and Chemical Engineering, Hunan University, Changsha 410082, P. R. China

Supporting Information

ABSTRACT: Blood glucose monitoring has attracted extensive attention because diabetes mellitus is a worldwide public health problem. Here, we reported an upconversion fluorescence detection method based on manganese dioxide (MnO_2)-nanosheet-modified upconversion nanoparticles (UCNPs) for rapid, sensitive detection of glucose levels in human serum and whole blood. In this strategy, MnO_2 nanosheets on the UCNP surface serve as a quencher. UCNP fluorescence can make a recovery by the addition of H_2O_2, which can reduce MnO_2 to Mn^{2+}, and the glucose can thus be monitored based on the enzymatic conversion of glucose by glucose oxidase to generate H_2O_2. Because of the nonautofluorescent assays offered by UCNPs, the developed method has been applied to monitor glucose levels in human serum and whole blood samples with satisfactory results. The proposed approach holds great potential for diabetes mellitus research and clinical diagnosis. Meanwhile, this nanosystem is also generalizable and can be easily expanded to the detection of various H_2O_2-involved analytes.

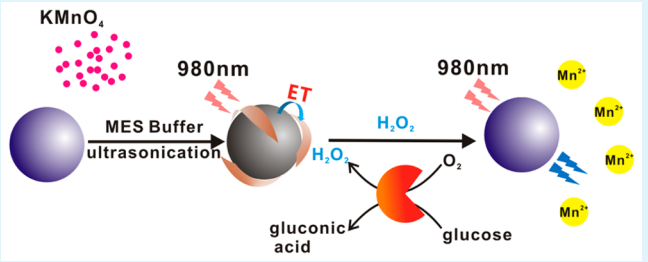

KEYWORDS: *lanthanide-doped upconversion nanoparticles, manganese dioxide, H_2O_2, glucose*

INTRODUCTION

Glucose is the major energy source in cellular metabolism and plays an essential role in the natural growth of cells. Glucose levels in blood are associated closely with diabetes or hypoglycemia. On the basis of the statistics of the World Health Organization, about 300 million people suffered from diabetes in the year 2010; this number is estimated to almost double in 2030. Thus, it is of great importance to be able to accurately monitor the blood glucose levels for the diagnosis and management of diabetes. Conventional methods for monitoring blood glucose levels are generally based on spectrophotometry,[1−7] fluorometry,[8−11] electrochemistry,[12−16] and chemiluminescence.[17,18] Although these methods are quite powerful, they are unsuitable for the direct monitoring of glucose levels in whole blood. The spectrophotometry- and electrochemistry-based methods are limited by the interference from blood color and contamination of the electrode by proteins in blood. Although the fluorometry-based ones can overcome the limitations, they commonly suffer from the autofluorescent background by UV−vis excitation light sources. Therefore, it is still highly desirable to develop technologies that are simple, sensitive, and low-cost and especially that can circumvent interferences from the complex whole blood samples for the diagnosis and management of diabetes.

The use of upconversion nanoparticles (UCNPs), which can convert near-infrared (NIR) excitation to visible emission, provides an alternative method for glucose monitoring.[19] In contrast to the conventional downconversion organic dyes and inorganic nanoparticles, UCNPs have exhibited attractive properties, such as sharp emission bandwidth, tunable multicolor emission, excellent photostability, enhanced light penetration depth, and negligible autofluorescence background interference.[20−28] These advantages make UCNPs particularly attractive for biolabeling and biosensing. In the past few years, several groups have developed UCNP-based Förster resonance energy transfer (FRET) techniques to detect ions,[29,30] small molecules,[31−33] protein,[34,35] and nucleic acids[36,37] by using various types of materials such as graphene oxide, organic dyes, and gold and carbon nanoparticles as acceptors. We have also developed a phospholipid-modified UCNP nanoprobe for ratiometric detection and imaging of phospholipase D[38] and a UCNP-based FRET biosensor for sensitive detection of the human immunodeficiency virus antibody in human serum.[39] Because of the negligible interference from autofluorescence of biological samples and scattering light under excitation of NIR light, it is expected that assays based on UCNPs can be used to directly monitor the glucose levels in whole blood.

Recently, Liu's group discovered that the fluorescence of UCNPs can be effectively quenched by MnO_2 nanosheets and the fluorescence can be turned on by adding a small amount of glutathione (GSH). They proposed a method based on MnO_2-modified UCNPs for quantification and imaging of GSH

Received: March 12, 2015
Accepted: April 28, 2015
Published: April 28, 2015

ACS Publications © 2015 American Chemical Society

DOI: 10.1021/acsami.5b02188
ACS Appl. Mater. Interfaces 2015, 7, 10548−10555

levels.[40] Interestingly, we found that the MnO_2-mediated quenching effect can also be reversed by adding a little H_2O_2. Presumably, the recovery of fluorescence may be attributed to the H_2O_2-mediated reduction of MnO_2 to Mn^{2+}, leading to decomposition of the MnO_2 nanosheets. On the basis of this finding, we proposed a MnO_2-modified upconversion nanosystem for the sensitive detection of glucose in blood based on the enzymatic conversion of glucose by glucose oxidase (GOx) to form H_2O_2. Compared with the previous glucose detection methods,[8−11] our present MnO_2-modified upconversion nanosystem has several outstanding features: first, the NIR-excitation technique offers nonautofluorescence assays, which enable the direct monitoring of glucose levels in whole blood; second, because of the negligible background interference resulting from NIR excitation, the proposed method has a lower detection limit than UV excitation; third, as the fluorescence report element, the high photostability of UCNPs can ensure ideal signal output. Therefore, this approach provides a sensitive, selective, and highly desirable blood glucose monitoring method.

EXPERIMENTAL SECTION

Reagents and Materials. Rare-earth chlorides $YCl_3·6H_2O$, $YbCl_3·6H_2O$, $(CH_2CO_2)_2Tm·xH_2O$, oleic acid (OA), NH_4F, NaOH, 1-octadecene (ODE; 90%), 2-(*N*-morpholino)ethanesulfonic acid (MES), glucose, glucose oxidase (GOx), lactate oxidase, L-tryptophan, L-phenylalanine, L-glutathione (L-GSH), and reduced *N*-ethylmaleimide (NEM) were purchased from Sigma-Aldrich. D-(+)-Maltose, D-fructose, D-(+)-galactose, L-lactic acid, and cysteine (Cys) were purchased from Sangon Biotech (Shanghai, China). L-Lysine, glycine, $KMnO_4$, NaH_2PO_4, Na_2HPO_4, NaCl, and other salts were purchased from Sinopharm Chemical Reagent Co., Ltd. (Shanghai, China).

Instruments. The transmission electron microscopy (TEM) images, powder X-ray diffraction (XRD) analysis, UV−vis absorption spectra, and upconversion luminescence spectra were all obtained by using the same instrumentation as those described in our previous literature.[38]

Synthesis of $NaYF_4$:Yb,Tm@$NaYF_4$ Core−Shell Nanoparticles. OA-capped $NaYF_4$:Yb,Tm core nanoparticles were first synthesized according to the method described by the literature with slight modification.[41] $YCl_3·6H_2O$ (0.695 mmol), $YbCl_3·6H_2O$ (0.30 mmol), and $(CH_2CO_2)_2Tm·xH_2O$ (0.005 mmol) (Y:Yb:Tm = 69.5:30:0.5 mole ratio) were added to a 50 mL three-necked flask containing OA (6 mL) and ODE (15 mL). The subsequent synthetic process was the same as that described in the literature reported by Zhao et al.[41] The resulting nanoparticles were precipitated by adding ethanol, collected by centrifugation at 5000 rpm for 5 min, washed several times with ethanol, and then dispersed in 2 mL of cyclohexane for the subsequent shell growth procedure. The $NaYF_4$:Yb,Tm@$NaYF_4$ core−shell nanoparticles were then synthesized. $YCl_3·6H_2O$ (1 mmol), octadecene (15 mL), and OA (6 mL) were added to a 50 mL three-necked flask. The shell growth process was also performed according to the literature reported by Zhao et al.[41] The obtained $NaYF_4$:Yb,Tm@$NaYF_4$ core−shell nanoparticles were dried under a vacuum for further experiments.

Preparation of Hydrophilic $NaYF_4$:Yb,Tm@$NaYF_4$ Core−Shell Nanoparticles. The azelaic acid capped hydrophilic nanoparticles were prepared according to the literature.[42] The as-prepared OA-capped $NaYF_4$:Yb,Tm@$NaYF_4$ core−shell nanoparticles (20 mg) dispersed in cyclohexane (1 mL) were added to a 100 mL two-necked flask containing cyclohexane (20 mL), *tert*-butyl alcohol (14 mL), water (2 mL), and an aqueous solution of K_2CO_3 (1 mL, 5 wt %). The resulting mixture was stirred for 20 min at room temperature. Then 4 mL of a Lemieux−von Rudloff reagent (5.7 mM $KMnO_4$ and 0.105 M $NaIO_4$ aqueous solutions) was dropwise added to the solution. Thereafter, the resulting mixture was stirred for 48 h at 40 °C. The product was collected by centrifugation and washed several times with deionized water, acetone, and ethanol. Subsequently, the product was treated with HCl (pH 4−5), and the mixture was stirred for 30 min at room temperature. At last, the product was centrifugated and washed and then redispersed in 6 mL of deionized water. The concentration of hydrophilic nanoparticles was calculated to be ∼3.0 mg mL^{-1}.

Preparation of MnO_2-Nanosheet-Modified $NaYF_4$:Yb,Tm@$NaYF_4$ Nanoparticles. MnO_2-nanosheet-modified nanoparticles were synthesized according to the method described by the literature.[40] In brief, an aqueous solution of azelaic acid capped hydrophilic $NaYF_4$:Yb,Tm@$NaYF_4$ core−shell nanoparticles (3.0 mg mL^{-1}, 100 μL) was first added to a 1.5 mL microcentrifuge tube. The subsequent preparation process was the same as that described in the literature reported by Liu et al.[40] The obtained MnO_2-nanosheet-modified nanoparticles were washed with deionized water to remove the excess potassium and free manganese ions and then redispersed in 1 mL of deionized water.

H_2O_2 Sensing. In a typical assay of H_2O_2, 50 μL of a MnO_2-nanosheet-modified UCNP aqueous solution (0.03 mg mL^{-1}) and different concentrations of H_2O_2 (40 μL) were added to 10 μL of 100 mM phosphate buffer (pH 7.0). The mixed solution was incubated at 37 °C for 40 min. Then, the upconversion fluorescence spectra were recorded under excitation of a 980 nm laser.

Glucose Detection. In a typical assay of glucose, 5 μL of 0.642 mg mL^{-1} GOx, 50 μL of a MnO_2-nanosheet-modified UCNP aqueous solution (0.03 mg mL^{-1}), and different concentrations of a glucose solution (35 μL) were added to 10 μL of 100 mM phosphate buffer (pH 7.0). The mixed solution was incubated at 37 °C for 40 min. Then, the upconversion fluorescence spectra were recorded under excitation of a 980 nm laser.

RESULTS AND DISCUSSION

Design and Principle for H_2O_2 and Glucose Detection Using MnO_2-Nanosheet-Modified UCNPs. The design strategy for H_2O_2 and glucose detection was based on H_2O_2 modulation of MnO_2-induced upconverted luminescence quenching of UCNPs (Scheme 1). To this end, $NaYF_4$:Yb,Tm@$NaYF_4$ core−shell nanocrystals with blue upconversion emission were synthesized and used as energy donors. The MnO_2 nanosheets were formed and coated on the surface of UCNPs through the reduction of $KMnO_4$ in MES buffer under sonication treatment. Because MnO_2 nanosheets have a broad absorption band from 250 to 500 nm,[40,43] which overlaps significantly with the blue emission of UCNPs, the upconverted luminescence of UCNPs can be effectively quenched by MnO_2 nanosheets coated on the surface of UCNPs. This MnO_2-induced quenching effect can be reversed by adding a small amount of H_2O_2. It would be the result of H_2O_2-mediated reduction of MnO_2 to Mn^{2+}, leading to decomposition of the

Scheme 1. Design and Principle for H_2O_2 and Glucose Detection Using a MnO_2-Nanosheet-Modified UCNP Nanocomposite

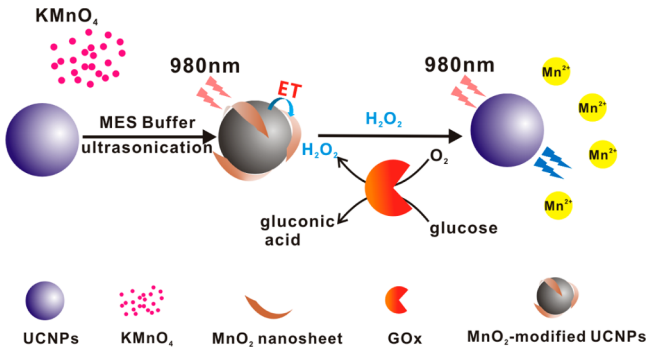

DOI: 10.1021/acsami.5b02188
ACS Appl. Mater. Interfaces 2015, 7, 10548−10555

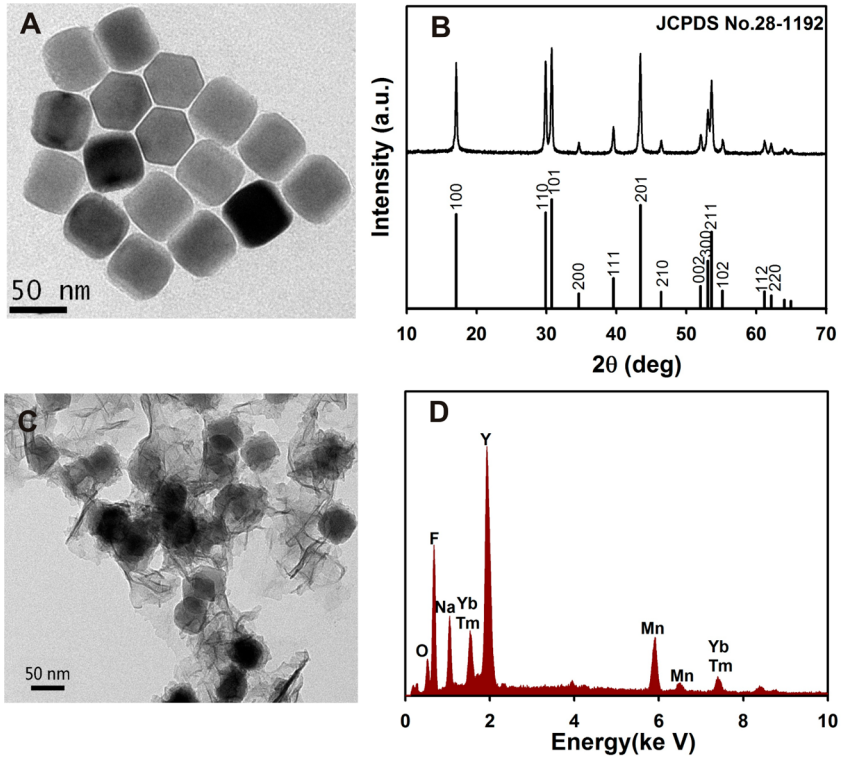

Figure 1. TEM image (A) and XRD patterns (B) of OA-capped $NaYF_4$:Yb,Tm@$NaYF_4$ core−shell UCNPs. TEM image (C) and EDS spectrum (D) of MnO_2-nanosheet-modified $NaYF_4$:Yb,Tm@$NaYF_4$ UCNP assemblies.

MnO_2 nanosheets accompanied by upconverted luminescence recovery. The reaction of MnO_2 to Mn^{2+} in the presence of a small amount of H_2O_2 can be represented as eq 1.[44]

$$MnO_2 + H_2O_2 + 2H^+ \rightarrow Mn^{2+} + 2H_2O + O_2 \quad (1)$$

Moreover, because glucose can be oxidized by oxygen (O_2) to produce H_2O_2 in the presence of GOx, a sensitive and cost-effective upconversion fluorescent assay can be achieved for monitoring of the blood glucose through the detection of enzymatically generated H_2O_2.

Synthesis and Characterization of UCNPs and MnO_2-Nanosheet-Modified UCNPs. Highly efficient upconverting $NaYF_4$:30%Yb,0.5%Tm@$NaYF_4$ core−shell nanoparticles were first prepared using the solvothermal method.[41] The TEM image showed that these nanocrystals displayed a uniform hexagonal platelike morphology with a mean size of approximately 50 nm in cyclohexane (Figure 1A). XRD analysis (Figure 1B) indicated that the obtained nanocrystals consisted of a hexagonal phase, whose peak positions and intensities agreed well with those of the pure hexagonal-phase $NaYF_4$:Yb,Tm nanocrystals (JCPDS no. 28-1192).

To prepare MnO_2-nanosheet-modified $NaYF_4$:Yb,Tm@$NaYF_4$ UCNPs, the OA ligand on the UCNP surface was first oxidized to azelaic acid according to a technique reported by Li et al.[42] The obtained azelaic acid capped UCNPs retained excellent monodispersion in water without changes in size, shape, and crystallinity after oxidation, as demonstrated by the TEM image (Figure S1 in the Supporting Information, SI). Dynamic light scattering (DLS) measurements showed a mean hydrodynamic diameter of approximately 55 nm for the azelaic acid capped UCNPs (Figure S2 in the SI), which was the same as that of OA-capped UCNPs dispersed in cyclohexane (ca. 55 nm), indicating that the oxidation process would not change the size of the UCNPs. Fourier transform infrared (FT-IR) spectra further demonstrated that the surface OA ligand was successfully oxidized to azelaic acid (Figure S3 in the SI). These results clearly confirmed that the hydrophilic nanoparticles were successfully prepared.

The hydrophilic $NaYF_4$:Yb,Tm@$NaYF_4$ UCNPs were then used to prepare the MnO_2-nanosheet-modified UCNPs by adding an aqueous $KMnO_4$ solution in the presence of MES buffer at pH 6. MES reduced $KMnO_4$ to form amorphous MnO_2 nanosheets on the surface of UCNPs. The formation of MnO_2-nanosheet-modified UCNP assemblies was confirmed by the TEM image (Figure 1C). Energy-dispersive X-ray spectroscopy (EDS) showed the signals of seven elements: Na, F, Y, Yb, Tm, Mn, and O (Figure 1D). Furthermore, in the X-ray photoelectron spectroscopy (XPS) analyses, two obvious Mn 2p peaks appeared at the spectra of MnO_2-modified hybrid nanomaterials (Figure S4 in the SI). These results verified the successful preparation of MnO_2-nanosheet-modified UCNP assemblies.

Next, the optical properties of UCNPs and MnO_2-modified UCNP assemblies were investigated. Under excitation of a 980 nm laser, the $NaYF_4$:Yb,Tm@$NaYF_4$ core−shell UCNPs exhibited four groups of emission lines, with maxima at 345, 360, 450, and 474 nm (Figure 2A). The MnO_2 nanosheets exhibited a broad absorption band centered at 370 nm, as shown by UV−vis absorption spectroscopy (Figures 2B and S5 in the SI), which matched well with the reported optical characteristics of MnO_2 nanomaterials.[40,43] This absorption may be due to d−d band transitions as described by previously reported literature.[45] The absorption of MnO_2 nanosheets showed a significant spectral overlap with the UV and blue emissions of the UCNPs, leading to FRET.

DOI: 10.1021/acsami.5b02188
ACS Appl. Mater. Interfaces 2015, 7, 10548−10555

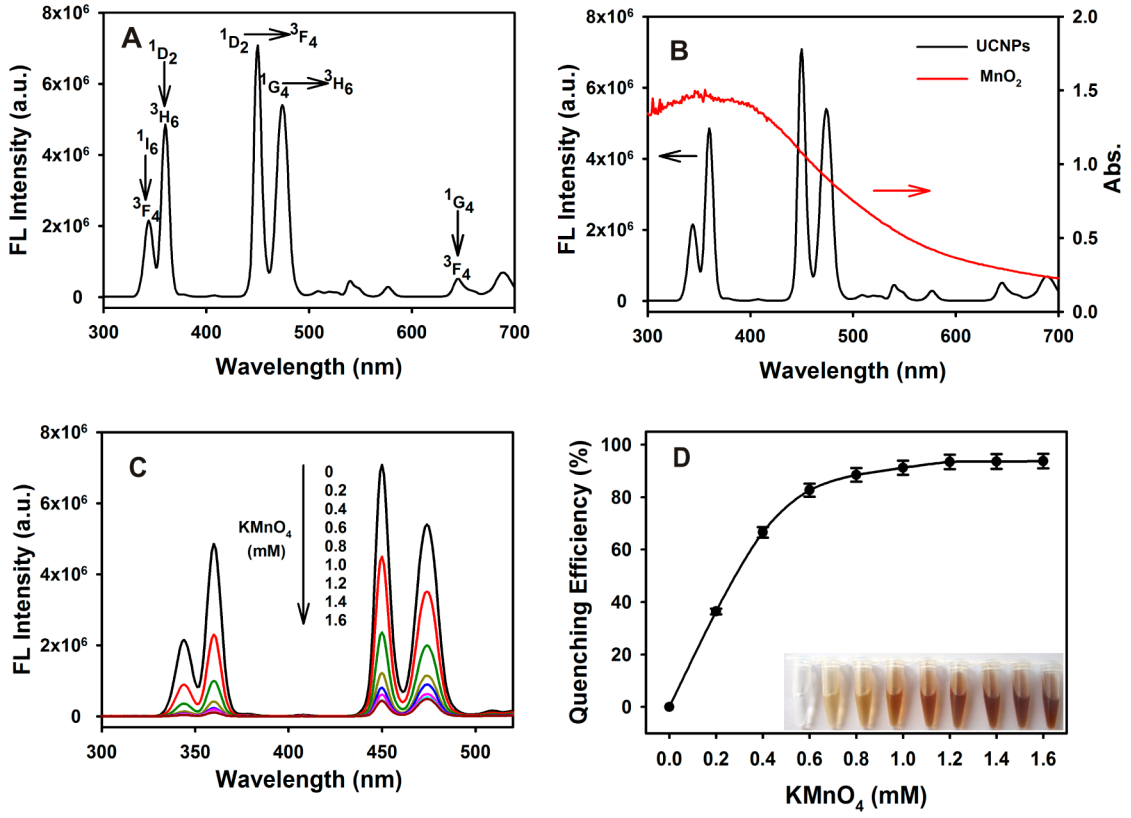

Figure 2. (A) Upconversion emission spectrum of $NaYF_4$:Yb,Tm@$NaYF_4$ core−shell UCNPs. (B) Absorption spectrum of MnO_2 nanosheets (red line) exhibiting significant spectral overlap with the emission spectrum of $NaYF_4$:Yb,Tm@$NaYF_4$ core−shell UCNPs under excitation of a 980 nm laser (black line). (C) Upconversion emission spectra of MnO_2-nanosheet-modified UCNP assemblies formed at a series of different $KMnO_4$ concentrations. The concentration of lanthanide ions was fixed at 0.3 mg mL^{-1}. (D) Relationship between the fluorescence quenching efficiency of MnO_2-modified UCNP assemblies at 450 nm and the $KMnO_4$ concentration. Inset: Photographs of the MnO_2-modified UCNP assembly aqueous solution formed at a series of different $KMnO_4$ concentrations.

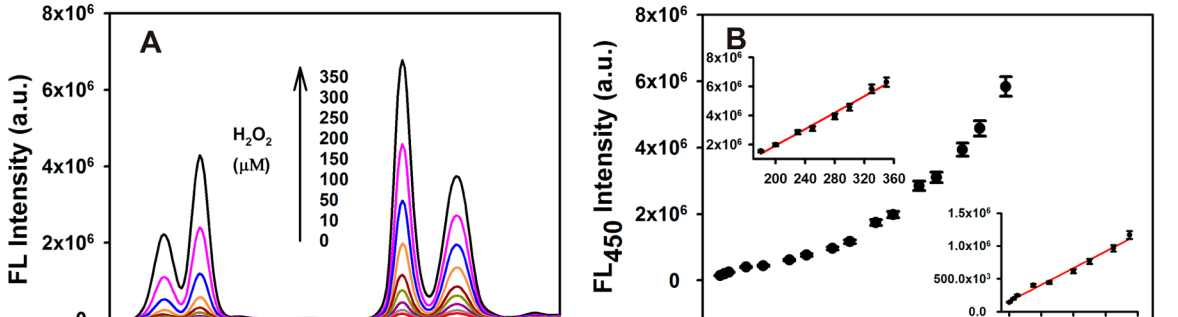

Figure 3. (A) Upconversion fluorescence response of MnO_2-nanosheet-modified $NaYF_4$:Yb,Tm@$NaYF_4$ UCNPs after incubation with H_2O_2 of different concentrations (0−350 μM) in phosphate buffer (pH 7.0). (B) Plot of the fluorescence intensity at 450 nm against the H_2O_2 concentration. Error bars indicate the standard deviations of three repetitive experiments.

In this work, MES was used to reduce $KMnO_4$ to form amorphous MnO_2 nanosheets on the surface of UCNPs. The effect of the $KMnO_4$ concentration on the quenching efficiency was studied in a fixed MES buffer. A series of MnO_2-modified UCNP assemblies were synthesized by changing $KMnO_4$ concentrations (from 0 to 1.6 mM). The upconversion fluorescence intensity of MnO_2-modified UCNP assemblies decreased gradually with increasing $KMnO_4$ concentrations (Figure 2C). Compared with the emission spectrum of UCNPs without MnO_2 modification, remarkable quenching (~93%) was obtained when 1.6 mM $KMnO_4$ was used. The influence of the $KMnO_4$ concentration on the quenching efficiency at 450 nm is shown in Figure 2D. The quenching efficiency was presented as $(F_0 - F)/F_0$, where F_0 and F represented the fluorescence intensity at 450 nm without and with MnO_2 modification, respectively. The quenching efficiency enhanced gradually with an increase in the $KMnO_4$ concentration and reached a maximum value of ~93% when 1.2 mM $KMnO_4$ was

DOI: 10.1021/acsami.5b02188
ACS Appl. Mater. Interfaces 2015, 7, 10548−10555

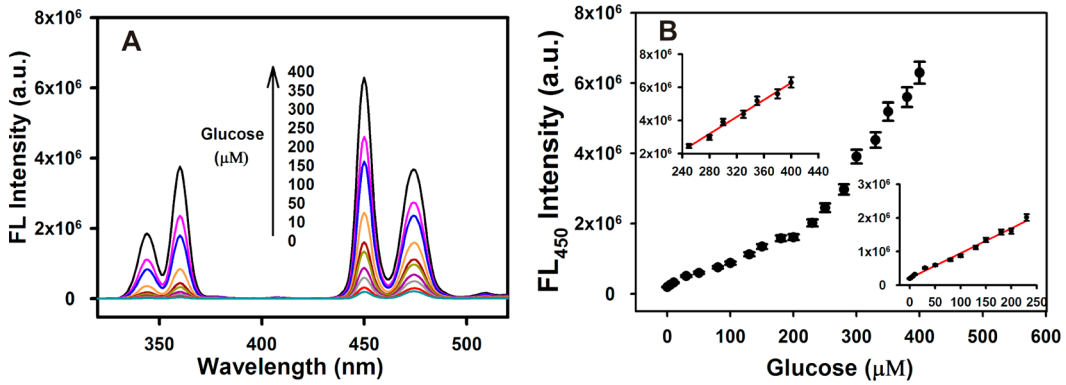

Figure 4. (A) Upconversion fluorescence response of MnO_2-nanosheet-modified $NaYF_4$:Yb,Tm@$NaYF_4$ UCNPs after incubation with glucose of different concentrations (0−400 μM) in phosphate buffer (pH 7.0) containing 0.0321 mg mL^{-1} GOx. (B) Plot of the fluorescence intensity at 450 nm against the glucose concentration. Error bars represent the standard deviation of three repetitive experiments.

used. In contrast, simple physical mixing of core−shell UCNPs and presynthesized MnO_2 nanosheets led to insignificant quenching (Figure S6 in the SI). This result further verified the FRET process from UCNPs to MnO_2 nanosheets. In addition, the TEM images of MnO_2-nanosheet-modified UCNPs formed at different $KMnO_4$ concentrations of 0.2, 0.6, and 1.2 mM are shown in Figure S7 in the SI. It can be seen from Figure S7 in the SI that the amount of MnO_2 nanosheets increased with increasing $KMnO_4$ concentrations. So, the number of MnO_2 nanosheets was one of the key factors that affected the quenching efficiency. Furthermore, it could be observed that the color of MnO_2-modified UCNP nanoassemblies became deeper with increasing $KMnO_4$ concentration (Figure 2D, inset). As a result, 1.2 mM $KMnO_4$ concentration was selected for the subsequent experiments.

H_2O_2 Sensing Based on MnO_2-Modified UCNPs. Having successfully synthesized the MnO_2-nanosheet-modified UCNPs, the possibility of H_2O_2 sensing using the hybrid nanoparticles was then explored. The reduction of MnO_2 to Mn^{2+} by H_2O_2 was first verified by a highly specific reaction for Mn^{2+} (Figure S8 in the SI). The purple solution and UV−vis absorption spectra that matched well with that of $KMnO_4$ from 450 to 600 nm clearly demonstrated the presence of Mn^{2+} after the reaction of MnO_2-modified UCNPs with H_2O_2. Next, we investigated the response of the MnO_2-modified UCNPs at different H_2O_2 concentrations. The upconversion fluorescence was gradually recovered with increasing concentration of H_2O_2 (Figure 3A). It was found that the upconversion fluorescence intensity of MnO_2-modified UCNPs further decreased from the original 499123 to 144460 after incubation in phosphate buffer (pH 7.0) at 37 °C for 40 min (the optimal experimental condition of H_2O_2 detection). The addition of 350 μM H_2O_2 caused a remarkable fluorescence signal (~6284010), corresponding to 43.5-fold enhancement, which indicated an almost complete recovery compared with that of UCNPs without MnO_2 modification. The recovery of upconversion fluorescence may be associated with the H_2O_2-mediated reduction of MnO_2 to Mn^{2+} (as shown in eq 1), which led to decomposition of the MnO_2 nanosheets. Figure 3B depicted the upconversion fluorescence intensity at 450 nm as a function of the H_2O_2 concentration. The fluorescence intensity at 450 nm was linearly correlated with the H_2O_2 concentration in the range of 0−150 μM (R^2 = 0.988) and 180−350 μM (R^2 = 0.987), respectively. The detection limit (in terms of the 3σ rule) was calculated to be 0.9 μM. Such a low detection limit can be attributed to the low background signal by NIR excitation.

Detection of Glucose Based on MnO_2-Modified UCNPs. Considering the significant importance of the monitoring of blood glucose levels for the diagnosis and management of diabetes, we further interrogated the feasibility of the MnO_2-modified UCNP nanocomposite for glucose detection. We first investigated the effect of the incubation temperature and reaction time on the fluorescence response (Figure S9 in the SI). The incubation temperature of 37 °C and reaction time of 40 min were selected for glucose detection in terms of the best signal-to-background ratio. In addition, the GOx concentration was also optimized. The responses at a series of GOx concentrations of 0.001284, 0.00642, 0.0128, 0.0321, 0.0642, and 0.1284 mg mL^{-1} under a maximum and fixed glucose concentration of 400 μM were recorded, and a GOx concentration of 0.0321 mg mL^{-1} was selected. The upconversion fluorescence intensity increased with increasing glucose concentration, varying from 0 to 400 μM (Figure 4A), and the fluorescence intensity at 450 nm was linearly related to the glucose concentration in the ranges of 0−250 μM (R^2 = 0.990) and 250−400 μM (R^2 = 0.985), respectively (Figure 4B). Presumably, the addition of a small amount of H_2O_2 (that is, at the low concentration of H_2O_2) mainly caused the dissociation of large MnO_2 nanosheets to form small nanosheets, and the latter still can quench the fluorescence of UCNPs, resulting in a relatively insignificant fluorescence recovery. In contrast, the addition of a large amount of H_2O_2 (that is, at the high concentration of H_2O_2) led to the complete dissociation of small MnO_2 nanosheets, generating significant fluorescence recovery. Therefore, the fluorescence intensity at 450 nm was linearly correlated with the H_2O_2 concentration in two separated ranges. The detection limit of the glucose was estimated to be 3.7 μM according to the 3σ rule. The MnO_2-modified UCNP nanosystem provided a lower detection limit than those reported by other optical methods for glucose detection.[4,7,11]

To further test the specificity of this nanosystem toward glucose, other possible interfering species including various saccharides, metal ions, proteins, and amino acids were incubated with a mixed solution of MnO_2-modified UCNPs and GOx. As shown in Figure 5, except for GSH and Cys, these species did not result in obvious interference in glucose detection. Because GSH and Cys could also reduce MnO_2 to Mn^{2+},[40] the upconversion fluorescence enhanced significantly

DOI: 10.1021/acsami.5b02188
ACS Appl. Mater. Interfaces 2015, 7, 10548−10555

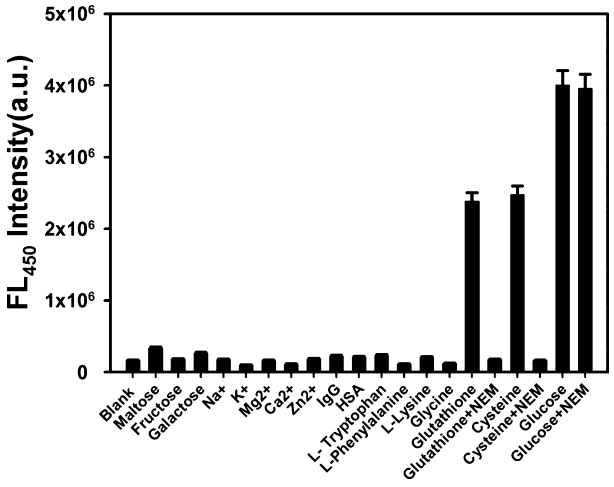

Figure 5. Upconversion fluorescence response at 450 nm of MnO_2-modified $NaYF_4$:Yb,Tm@$NaYF_4$ nanoparticle solutions in the presence of different saccharides, metal ions, proteins, and amino acids (3 mM each). The concentrations of GSH, Cys, and glucose were 0.3 mM, and the NEM concentration was 0.9 mM. Error bars represent the standard deviations of three repetitive experiments.

after the addition of GSH and Cys. However, the interference of GSH and Cys could be eliminated by adding NEM, a scavenger that can specifically react with GSH and Cys.[46] As can be seen from Figure 5, after incubation of GSH or Cys with NEM, the addition of MnO_2-modified UCNPs gave a negligible signal enhancement, whereas glucose detection was unaffected by the introduction of NEM. Therefore, by using NEM as an effective scavenger of GSH and Cys, the MnO_2-modified UCNP nanosystem can provide a highly selective and sensitive upconversion approach for glucose detection.

To evaluate the feasibility of the MnO_2-modified UCNP nanosystem for glucose detection in biological samples, the developed method was applied to detect five individual real samples including three human serum samples and two whole blood samples. Taking into consideration the normal glucose level in healthy human blood as well as the linear range of our method, 5 μL of samples was added to the reaction system and diluted to 100 μL, which was a 20-fold dilution. NEM (0.3 mM) was added to the samples to eliminate the interference from GSH and Cys in real samples. After the addition of 0.3 mM NEM to the human serum sample, the upconversion fluorescence intensity of MnO_2-modified UCNPs in human serum decreased obviously, and the obtained spectrum was almost the same as that in phosphate buffer (Figure S10 in the SI), indicating that NEM did eliminate the interference of GSH and Cys in blood samples. The analytical results are presented in Table 1. The glucose concentrations of the clinical samples were within the range of 4.4−6.6 mM, which was consistent with the reported levels.[12] In addition, standard addition experiments were also carried out. The recoveries ranged from 96.0% to 104.5% for the five real samples, and a relative standard deviation (RSD) of around 5% was obtained. These results have demonstrated the applicability of this MnO_2-modified UCNP nanosystem for blood glucose monitoring in real samples.

Generality of the MnO_2-Nanosheet-Modified UCNP Nanosystem. To investigate the generality of the MnO_2-modified UCNP nanosystem, the proposed strategy was also applied to the detection of L-lactic acid. It is well-known that lactate oxidase can catalyze the oxidation of L-lactic acid to generate pyruvate and H_2O_2, and L-lactic acid can be assayed through the detection of enzymatically generated H_2O_2. As shown in Figure S11 in the SI, the upconversion fluorescence intensity increased with increasing L-lactic acid concentration, varying from 0 to 800 μM, and the fluorescence intensity at 450 nm was linearly related to the L-lactic acid concentration in the ranges of 50−400 μM (R^2 = 0.986) and 450−800 μM (R^2 = 0.967), with a detection limit of 10 μM. This result has demonstrated that the MnO_2-modified UCNP nanosystem is generalizable and can be applied to the detection of various H_2O_2-involved analytes.

Table 1. Determination of the Glucose Levels in Human Serum and Whole Blood Samples Using the MnO_2-Modified UCNP Nanosystem

sample[α]	measured (mM)	added (mM)	found (mM)	recovery (%)	RSD (%)
1	4.95	1.00	5.80	97.5	3.3
2	6.50	1.00	7.84	104.5	2.9
3	5.78	1.00	6.85	101.0	4.0
4	5.45	1.00	6.19	96.0	5.3
5	4.58	1.00	5.50	98.6	4.1

[α]Samples 1−3 were human serum, and samples 4 and 5 were whole blood.

CONCLUSIONS

We have developed a novel method based on MnO_2-nanosheet-modified UCNPs for rapid monitoring of blood glucose levels. By combining the highly sensitive H_2O_2/MnO_2 reaction with the nonautofluorescent advantage of UCNPs, a highly sensitive, selective, and cost-efficient sensing approach for glucose detection has been designed and applied to monitor glucose levels in human serum and whole blood samples with satisfactory results. The proposed nanosystem has great potential for diabetes mellitus research and clinical diagnosis. Meanwhile, this nanosystem is also generalizable and can be easily extended to the detection of various H_2O_2-involved analytes. The proposed strategy may offer a new approach to developing low-cost and sensitive methods for biological and clinical diagnostics applications.

ASSOCIATED CONTENT

Supporting Information

Additional information as noted in the text, including experimental details of L-lactic acid and Mn^{2+} detection, TEM image of azelaic acid capped UCNPs, DLS and FT-IR spectra of OA-capped and azelaic acid-capped UCNPs, XPS spectra of UCNPs and MnO_2-nanosheet-modified UCNPs, UV−vis absorption spectra of $KMnO_4$, MnO_2 nanosheets, UCNPs, and MnO_2-nanosheet-modified UCNPs, upconversion emission spectra of UCNPs, a mixing solution of UCNPs and presynthesized MnO_2 nanosheets, and MnO_2-nanosheet-modified UCNPs, TEM images of MnO_2-modified UCNPs formed at different $KMnO_4$ concentrations (0.2, 0.6, and 1.2 mM), demonstration of the reduction of MnO_2 to Mn^{2+} by H_2O_2, effects of the incubation temperature and reaction time on the fluorescence responses of MnO_2-modified UCNPs to 100 μM glucose, the effect of NEM on glucose detection in human serum, and upconversion fluorescence response of MnO_2-modified UCNPs to L-lactic acid of varying concentrations. The Supporting Information is available free of charge

DOI: 10.1021/acsami.5b02188
ACS Appl. Mater. Interfaces 2015, 7, 10548−10555

on the ACS Publications website at DOI: 10.1021/acsami.5b02188.

AUTHOR INFORMATION

Corresponding Author

*E-mail: xiachu@hnu.edu.cn. Tel.: 86-731-88821916. Fax: 86-731-88821916.

Notes

The authors declare no competing financial interest.

ACKNOWLEDGMENTS

This work was supported by the National Natural Science Foundation of China (Grant 21275045), NCET-11-0121, and Hunan Provincial Natural Science Foundation of China (Grant 12JJ1004).

REFERENCES

(1) Sanz, V.; De Marcos, S.; Castillo, J. R.; Galbán, J. Application of Molecular Absorption Properties of Horseradish Peroxidase for Self-Indicating Enzymatic Interactions and Analytical Methods. *J. Am. Chem. Soc.* **2005**, *127*, 1038−1048.

(2) Chen, S.; Hai, X.; Chen, X. W.; Wang, J. H. In Situ Growth of Silver Nanoparticles on Graphene Quantum Dots for Ultrasensitive Colorimetric Detection of H_2O_2 and Glucose. *Anal. Chem.* **2014**, *86*, 6689−6694.

(3) Ornatska, M.; Sharpe, E.; Andreescu, D.; Andreescu, S. Paper Bioassay Based on Ceria Nanoparticles as Colorimetric Probes. *Anal. Chem.* **2011**, *83*, 4273−4280.

(4) Wei, H.; Wang, E. Fe_3O_4 Magnetic Nanoparticles as Peroxidase Mimetics and Their Applications in H_2O_2 and Glucose Detection. *Anal. Chem.* **2008**, *80*, 2250−2254.

(5) Shi, W.; Wang, Q.; Long, Y.; Cheng, Z.; Chen, S.; Zheng, H.; Huang, Y. Carbon Nanodots as Peroxidase Mimetics and Their Applications to Glucose Detection. *Chem. Commun.* **2011**, *47*, 6695−6697.

(6) Chen, Q.; Liu, M.; Zhao, J.; Peng, X.; Chen, X.; Mi, N.; Yin, B.; Li, H.; Zhang, Y.; Yao, S. Water-Dispersible Silicon Dots as a Peroxidase Mimetic for the Highly-Sensitive Colorimetric Detection of Glucose. *Chem. Commun.* **2014**, *50*, 6771−6774.

(7) Radhakumary, C.; Sreenivasan, K. Naked Eye Detection of Glucose in Urine Using Glucose Oxidase Immobilized Gold Nanoparticles. *Anal. Chem.* **2011**, *83*, 2829−2833.

(8) Li, L.; Gao, F.; Ye, J.; Chen, Z.; Li, Q.; Gao, W.; Ji, L.; Zhang, R.; Tang, B. FRET-Based Biofriendly Apo-GOx-Modified Gold Nanoprobe for Specific and Sensitive Glucose Sensing and Cellular Imaging. *Anal. Chem.* **2013**, *85*, 9721−9727.

(9) Wu, P.; He, Y.; Wang, H. F.; Yan, X. P. Conjugation of Glucose Oxidase onto Mn-Doped ZnS Quantum Dots for Phosphorescent Sensing of Glucose in Biological Fluids. *Anal. Chem.* **2010**, *82*, 1427−1433.

(10) Shen, P.; Xia, Y. Synthesis-Modification Integration: One-Step Fabrication of Boronic Acid Functionalized Carbon Dots for Fluorescent Blood Sugar Sensing. *Anal. Chem.* **2014**, *86*, 5323−5329.

(11) Jin, L.; Shang, L.; Guo, S.; Fang, Y.; Wen, D.; Wang, L.; Yin, J.; Dong, S. Biomolecule-Stabilized Au Nanoclusters as a Fluorescence Probe for Sensitive Detection of Glucose. *Biosens. Bioelectron.* **2011**, *26*, 1965−1969.

(12) Wang, J. Electrochemical Glucose Biosensors. *Chem. Rev.* **2008**, *108*, 814−825.

(13) Zhai, D.; Liu, B.; Shi, Y.; Pan, L.; Wang, Y.; Li, W.; Zhang, R.; Yu, G. Highly Sensitive Glucose Sensor Based on Pt Nanoparticle/Polyaniline Hydrogel Heterostructures. *ACS Nano* **2013**, *7*, 3540−3546.

(14) Song, J.; Xu, L.; Zhou, C.; Xing, R.; Dai, Q.; Liu, D.; Song, H. Synthesis of Graphene Oxide Based CuO Nanoparticles Composite Electrode for Highly Enhanced Nonenzymatic Glucose Detection. *ACS Appl. Mater. Interfaces* **2013**, *5*, 12928−12934.

(15) Lin, L.; Yan, J.; Li, J. Small-Molecule Triggered Cascade Enzymatic Catalysis in Hour-Glass Shaped Nanochannel Reactor for Glucose Monitoring. *Anal. Chem.* **2014**, *86*, 10546−10551.

(16) Liu, Q.; Lu, X.; Li, J.; Yao, X.; Li, J. Direct Electrochemistry of Glucose Oxidase and Electrochemical Biosensing of Glucose on Quantum Dots/Carbon Nanotubes Electrodes. *Biosens. Bioelectron.* **2007**, *22*, 3203−3209.

(17) Bostick, D. T.; Hercules, D. M. Quantitative Determination of Blood Glucose Using Enzyme Induced Chemiluminescence of Luminsl. *Anal. Chem.* **1975**, *47*, 447−452.

(18) Lan, D.; Li, B.; Zhang, Z. Chemiluminescence Flow Biosensor for Glucose Based on Gold Nanoparticle-Enhanced Activities of Glucose Oxidase and Horseradish Peroxidase. *Biosens. Bioelectron.* **2008**, *24*, 934−938.

(19) Haase, M.; Schäfer, H. Upconverting Nanoparticles. *Angew. Chem., Int. Ed.* **2011**, *50*, 5808−5829.

(20) Wang, G.; Peng, Q.; Li, Y. Lanthanide-Doped Nanocrystals: Synthesis, Optical-Magnetic Properties, and Applications. *Acc. Chem. Res.* **2011**, *44*, 322−332.

(21) Wang, F.; Liu, X. Upconversion Multicolor Fine-Tuning: Visible to Near-Infrared Emission from Lanthanide-Doped $NaYF_4$ Nanoparticles. *J. Am. Chem. Soc.* **2008**, *130*, 5642−5643.

(22) Mader, H. S.; Kele, P.; Saleh, S. M.; Wolfbeis, O. S. Upconverting Luminescent Nanoparticles for Use in Bioconjugation and Bioimaging. *Curr. Opin. Chem. Biol.* **2010**, *14*, 582−596.

(23) Wu, S. W.; Han, G.; Milliron, D. J.; Aloni, S.; Altoe, V.; Talapin, D. V.; Cohen, B. E.; Schuck, P. J. Non-Blinking and Photostable Upconverted Luminescence from Single Lanthanide-Doped Nanocrystals. *Proc. Natl. Acad. Sci. U.S.A.* **2009**, *106*, 10917−10921.

(24) Dong, Y. B.; Wang, P.; Ma, J. P.; Zhao, X. X.; Wang, H. Y.; Tang, B.; Huang, R. Q. Coordination-Driven Nanosized Lanthanide "Molecular Lantern" with Tunable Luminescent Properties. *J. Am. Chem. Soc.* **2007**, *129*, 4872−4873.

(25) Wang, F.; Liu, X. Multicolor Tuning of Lanthanide-Doped Nanoparticles by Single Wavelength Excitation. *Acc. Chem. Res.* **2014**, *47*, 1378−1385.

(26) Auzel, F. Upconversion and Anti-Stokes Processes with f and d Ions in Solids. *Chem. Res.* **2004**, *104*, 139−174.

(27) Li, L. L.; Wu, P.; Hwang, K.; Lu, Y. An Exceptionally Simple Strategy for DNA-Functionalized Up-Conversion Nanoparticles as Biocompatible Agents for Nanoassembly, DNA Delivery, and Imaging. *J. Am. Chem. Soc.* **2013**, *135*, 2411−2414.

(28) Li, L. L.; Zhang, R.; Yin, L.; Zheng, K.; Qin, W.; Selvin, P. R.; Lu, Y. Biomimetic Surface Engineering of Lanthanide-Doped Upconversion Nanoparticles as Versatile Bioprobes. *Angew. Chem., Int. Ed.* **2012**, *51*, 6121−6125.

(29) Liu, Q.; Peng, J.; Sun, L.; Li, F. High-Efficiency Upconversion Luminescent Sensing and Bioimaging of Hg(II) by Chromophoric Ruthenium Complex-Assembled Nanophosphors. *ACS Nano* **2011**, *5*, 8040−8048.

(30) Li, Z.; Lv, S.; Wang, Y.; Chen, S.; Liu, Z. Construction of LRET-Based Nanoprobe Using Upconversion Nanoparticles with Confined Emitters and Bared Surface as Luminophore. *J. Am. Chem. Soc.* **2015**, *137*, 3421−3427.

(31) Xiao, Y.; Zeng, L.; Xia, T.; Wu, Z.; Liu, Z. Construction of an Upconversion Nanoprobe with Few-Atom Silver Nanoclusters as the Energy Acceptor. *Angew. Chem., Int. Ed.* **2015**, *54*, DOI: 10.1002/anie.201500008.

(32) Zhang, C.; Yuan, Y.; Zhang, S.; Wang, Y.; Liu, Z. Biosensing Platform Based on Fluorescence Resonance Energy Transfer from Upconverting Nanocrystals to Graphene Oxide. *Angew. Chem., Int. Ed.* **2011**, *50*, 6851−6854.

(33) Achatz, D. E.; Meier, R. J.; Fischer, L. H.; Wolfbeis, O. S. Luminescent Sensing of Oxygen Using a Quenchable Probe and Upconverting Nanoparticles. *Angew. Chem., Int. Ed.* **2011**, *50*, 260−263.

(34) Wang, Y.; Bao, L.; Liu, Z.; Pang, D. W. Aptamer Biosensor Based on Fluorescence Resonance Energy Transfer from Upconvert-

ing Phosphors to Carbon Nanoparticles for Thrombin Detection in Human Plasma. *Anal. Chem.* **2011**, *83*, 8130−8137.
(35) Wang, Y.; Shen, P.; Li, C.; Wang, Y.; Liu, Z. Upconversion Fluorescence Resonance Energy Transfer Based Biosensor for Ultrasensitive Detection of Matrix Metalloproteinase-2 in Blood. *Anal. Chem.* **2012**, *84*, 1466−1473.
(36) Zhang, P.; Rogelj, S.; Nguyen, K.; Wheeler, D. Design of a Highly Sensitive and Specific Nucleotide Sensor Based on Photon Upconverting Particles. *J. Am. Chem. Soc.* **2006**, *128*, 12410−12411.
(37) Wu, S.; Duan, N.; Shi, Z.; Fang, C.; Wang, Z. Simultaneous Aptasensor for Multiplex Pathogenic Bacteria Detection Based on Multicolor Upconversion Nanoparticles Labels. *Anal. Chem.* **2014**, *86*, 3100−3107.
(38) Cen, Y.; Wu, Y. M.; Kong, X. J.; Wu, S.; Yu, R. Q.; Chu, X. Phospholipid-Modified Upconversion Nanoprobe for Ratiometric Fluorescence Detection and Imaging of Phospholipase D in Cell Lysate and in Living Cells. *Anal. Chem.* **2014**, *86*, 7119−7127.
(39) Wu, Y. M.; Cen, Y.; Huang, L. J.; Yu, R. Q.; Chu, X. Upconversion Fluorescence Resonance Energy Transfer Biosensor for Sensitive Detection of Human Immunodeficiency Virus Antibodies in Human Serum. *Chem. Commun.* **2014**, *50*, 4759−4762.
(40) Deng, R.; Xie, X.; Vendrell, M.; Chang, Y. T.; Liu, X. Intracellular Glutathione Detection Using MnO_2-Nanosheet-Modified Upconversion Nanoparticles. *J. Am. Chem. Soc.* **2011**, *133*, 20168−20171.
(41) Yan, B.; Boyer, J. C.; Branda, N. R.; Zhao, Y. Near-Infrared Light-Triggered Dissociation of Block Copolymer Micelles Using Upconverting Nanoparticles. *J. Am. Chem. Soc.* **2011**, *133*, 19714−19717.
(42) Chen, Z.; Chen, H.; Hu, H.; Yu, M.; Li, F.; Zhang, Q.; Zhou, Z.; Yi, T. Versatile Synthesis Strategy for Carboxylic Acid-functionalized Upconverting Nanophosphors as Biological Labels. *J. Am. Chem. Soc.* **2008**, *130*, 3023−3029.
(43) Zhang, X. L.; Zheng, C.; Guo, S. S.; Li, J.; Yang, H. H.; Chen, G. Turn-On Fluorescence Sensor for Intracellular Imaging of Glutathione Using g-C3N4 Nanosheet-MnO_2 Sandwich Nanocomposite. *Anal. Chem.* **2014**, *86*, 3426−3434.
(44) Nakayama, M.; Sato, A.; Yamaguchi, R. Decomposition and Detection of Hydrogen Peroxide Using d-MnO_2 Thin Film Electrode with Self-Healing Property. *Electroanalysis* **2013**, *25*, 2283−2288.
(45) Omomo, Y.; Sasaki, T.; Wang, L.; Watanabe, M. Redoxable Nanosheet Crystallites of MnO_2 Derived via Delamination of a Layered Manganese Oxide. *J. Am. Chem. Soc.* **2003**, *125*, 3568−3575.
(46) Gregory, J. D. The Stability of *N*-Ethylmaleimide and its Reaction with Sulfhydryl Groups. *J. Am. Chem. Soc.* **1955**, *77*, 3922−3923.

DOI: 10.1021/acsami.5b02188
ACS Appl. Mater. Interfaces 2015, 7, 10548−10555